



## Importance of the Fermi surface and magnetic interactions for the superconducting dome in electron-doped FeSe intercalates

Makoto Shimizu,<sup>1</sup> Nayuta Takemori ,<sup>2</sup> Daniel Guterding ,<sup>3</sup> and Harald O. Jeschke <sup>2</sup>

<sup>1</sup>*Department of Physics, Okayama University, Okayama 700-8530, Japan*

<sup>2</sup>*Research Institute for Interdisciplinary Science, Okayama University, Okayama 700-8530, Japan*

<sup>3</sup>*Fachbereich Mathematik, Naturwissenschaften und Datenverarbeitung, Technische Hochschule Mittelhessen, Wilhelm-Leuschner-Straße 13, 61169 Friedberg, Germany*



(Received 8 March 2020; revised manuscript received 13 May 2020; accepted 13 May 2020; published 27 May 2020)

The van-der-Waals gap of iron chalcogenide superconductors can be intercalated with a variety of inorganic and organic compounds that modify the electron doping level of the iron layers. In  $\text{Li}_x(\text{C}_3\text{N}_2\text{H}_{10})_{0.37}\text{FeSe}$ , a dome in the superconducting transition temperature  $T_c$  has been reported to occur in the doping range of  $x = 0.06$  to  $x = 0.68$ . We use a combination of density functional theory and spin fluctuation theory to capture the evolution of superconducting transition temperatures theoretically. We clearly demonstrate how the changing electronic structure supports an increasing superconducting  $T_c$ . The suppression of  $T_c$  at high doping levels can, however, only be understood by analyzing the magnetic tendencies, which evolve from stripe-type at low doping to bicollinear at high doping.

DOI: [10.1103/PhysRevB.101.180511](https://doi.org/10.1103/PhysRevB.101.180511)

**Introduction.** Iron chalcogenide superconductors, while structurally simple, have emerged as one of the most interesting and electronically most complicated of the various families of iron-based superconductors [1–3]. FeSe, in particular, is intensely studied due to its nematic phase which occurs in a very large temperature range [4] and due to its peculiar electronic structure that is not correctly captured by any known electronic structure technique [5]. After the discovery of superconducting FeSe [6] it was realized that the superconducting transition temperatures can be significantly enhanced if the van der Waals gap between the iron selenium layers is intercalated with alkali metal ions, for example by the ammonia technique [7–10] or directly in the structurally complicated  $A_x\text{Fe}_{2-y}\text{Se}_2$  type of compounds with  $A = \text{K}, \text{Rb}, \text{Cs}$  [11,12]. Further possibilities are completely inorganic lithium hydroxide intercalates [13,14] and alkali metal intercalates stabilized by organic solvents [15]. Not only FeSe but also FeS [16] and  $\text{FeSe}_{1-x}\text{Te}_x$  [17,18] can be intercalated.

At least three tuning parameters have been identified that provide control over the superconducting transition temperature: Pressure can increase the  $T_c$  of bulk FeSe from 8 K at ambient pressure to 36.7 K [19]. By electron doping via lithium and ammonia intercalation,  $T_c$  up to 55 K can be reached [10]. The spacing between FeSe layers can be systematically increased using amines of increasing size, like ethylenediamine ( $\text{C}_2\text{H}_8\text{N}_2$ ) [15,20], 2-phenethylamine ( $\text{C}_3\text{H}_{11}\text{N}$ ) [21], diaminopropane ( $\text{C}_3\text{H}_{10}\text{N}_2$ ) [20,22], hexamethylenediamine ( $\text{C}_6\text{H}_{16}\text{N}_2$ ) [23,24], and  $T_c$  up to 41 K has been observed [24].

Tuning parameters can also be combined, for example by pressurizing doped FeSe intercalates [25–28]. When parameters like pressure or doping, which can be varied continuously, are tuned away from their optimal values, characteristic superconducting domes are observed [25–29].

Here, we are interested in finding microscopic explanations for superconducting domes, also in the hope of discovering ways to manipulate and increase transition temperatures. Theoretically, superconductivity in iron-based materials has been tackled from a weak coupling perspective, describing Fermi surface instabilities that lead to superconductivity via spin fluctuations [30–32], and from a strong coupling picture by considering these materials as doped Mott insulators, where superconductivity is obtained from approximately solved  $t$ - $J$  models [33–35]. However, capturing superconducting  $T_c$  trends continues to be a theoretical challenge [36]. Within a spin fluctuation scenario, the  $T_c$  increase with doping has been explained for lithium ammonia intercalated FeSe [37], and for FeS, a pressure induced double dome was captured [38]. The dispute between itinerant and localized electron pictures is ongoing, and while some iron-based superconductor families, like 1111, are more itinerant, others, like hole doped 122 and iron chalcogenides are more localized. In fact, superconductivity can be shown to depend both on Fermi surface shape and antiferromagnetic exchange [39]. Even in the absence of a magnetic ground state, the nature of the magnetic exchange has important implications for nematicity and superconductivity in FeSe [40] and for the differences between iron pnictides and germanides [41].

In this Rapid Communication, we will focus on the lithium diaminopropane intercalated material  $\text{Li}_x(\text{C}_3\text{N}_2\text{H}_{10})_{0.37}\text{FeSe}$  where charge doping has been controlled experimentally in a wide range  $0.06 \leq x \leq 0.68$  [22]. We will work both in the itinerant scenario by applying spin fluctuation theory and in the localized picture by working out the consequences of the Heisenberg interactions. We will show that the underdoped side of the superconducting dome can be well understood based on Fermi surfaces, but in order to explain the decreasing

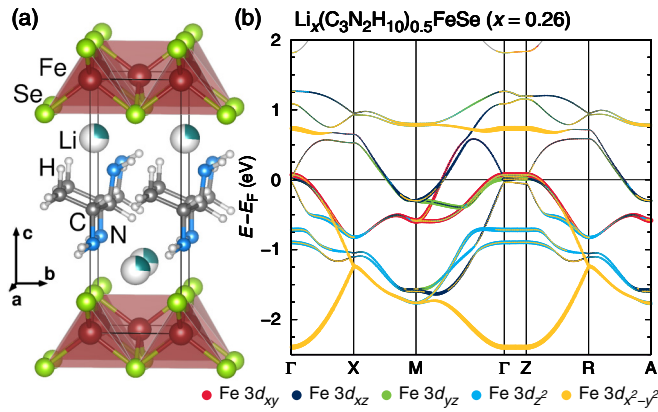


FIG. 1. (a) Crystal structure of  $\text{Li}_x(\text{C}_3\text{N}_2\text{H}_{10})_{0.5}\text{FeSe}$ ; the Li position is only 26% occupied, indicated by partial coloring. (b) Corresponding bands near the Fermi level  $E_F$  with Fe 3d orbital weights.

$T_c$  at high doping, we need to evoke the high energy argument that, with increasing carrier density, magnetic interactions mutate from FeSe-like to FeTe-like.

**Methods.** We study the electronic structure of  $\text{Li}_x(\text{C}_3\text{N}_2\text{H}_{10})_{0.5}\text{FeSe}$  as a function of doping by performing a series of density functional theory (DFT) calculations within the full-potential local orbital (FPLO) [42] basis, using the generalized gradient approximation (GGA) exchange correlation functional [43] and  $24 \times 24 \times 24$   $k$  mesh. We construct tight-binding models including all ten Fe 3d orbitals using projective Wannier functions [44]. Using the glide reflection unfolding technique [45], we turn the ten-band into a five-band model. We calculate the noninteracting susceptibility  $\chi_0$  on a  $50 \times 50 \times 10$   $q$  mesh. We employ the random phase approximation (RPA) to calculate spin and charge susceptibilities and solve a gap equation to obtain pairing symmetry  $\Delta$  and eigenvalue  $\lambda$  [46,47]. On the other hand, we use the energy mapping method to measure the exchange interactions of  $\text{Li}_x(\text{C}_3\text{N}_2\text{H}_{10})_{0.5}\text{FeSe}$  [41,48,49] and iterative minimization to find ground state spin configurations for the calculated Hamiltonians [50,51].

**Results.** We first generate a sequence of crystal structures for  $\text{Li}_x(\text{C}_3\text{N}_2\text{H}_{10})_{0.37}\text{FeSe}$  based on the structural data determined by Sun *et al.* [22]. We smoothly interpolate the structural data for the lattice parameters and the FeSe layer (see Ref. [51] for details, in particular Fig. S1) and simplify the disordered diaminopropane molecules to a single molecule per two FeSe, yielding the composition  $\text{Li}_x(\text{C}_3\text{N}_2\text{H}_{10})_{0.5}\text{FeSe}$  shown in Fig. 1(a). We mount the  $\text{C}_3\text{N}_2\text{H}_{10}$  molecule with fixed geometry into the entire structure sequence, since bond lengths and angles of a neutral molecule should not be affected by the charging and contraction of the FeSe layer (see Ref. [51] for further details). An example of the DFT electronic structure with Fe 3d weights is shown in Fig. 1(b). Calculations for the complete sequence of structures without diaminopropane molecule, in  $P4/nmm$  symmetry, yield similar results [51].

We first quantify the charge doping by integration of Fe 3d total and partial electron densities. We find that the charge  $-xe$  provided by  $\text{Li}_x^+$  is indeed fully doping the Fe plane; Fe charge evolves almost linearly from  $n_{3d}^{\text{total}} = 6.06$  to 6.65 in the

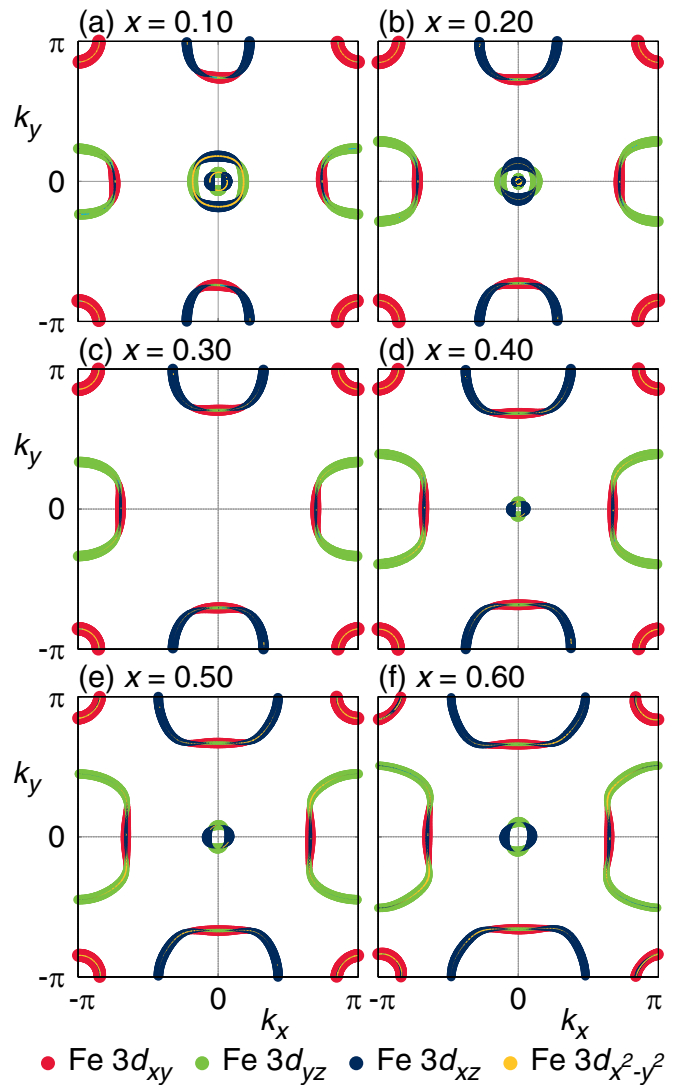


FIG. 2. Evolution of the Fermi surface of  $\text{Li}_x(\text{C}_3\text{N}_2\text{H}_{10})_{0.5}\text{FeSe}$  at  $k_z = 0$  with doping. The Fe 3d orbital weights are indicated by color. Orbital weight of Fe  $3d_{z^2}$  at the Fermi level is nearly negligible.

interval  $0.06 < x < 0.68$  (see Ref. [51], Fig. S2). The orbital with strongest charge increase is  $d_{xy}$ , followed by  $d_{xz}/d_{yz}$ .

The decisive factor in spin fluctuation theory is Fermi surfaces. We show in Fig. 2 the unfolded one iron Fermi surfaces of  $\text{Li}_x(\text{C}_3\text{N}_2\text{H}_{10})_{0.5}\text{FeSe}$  for six doping levels (see Fig. S3 of Ref. [51] for the same without  $\text{C}_3\text{N}_2\text{H}_{10}$  molecules). First of all, we note that the overall number and size of Fermi surface pockets are in good agreement with those observed by angle resolved photoemission in the related FeSe intercalates ( $\text{Li}_{0.84}\text{Fe}_{0.16}\text{OHFe}_{0.98}\text{Se}$  and  $(\text{Tl}, \text{Rb})_x\text{Fe}_{2-y}\text{Se}_2$  (see Fig. 1 of Ref. [55]). Even though we do not know the precise doping levels of those compounds, the overall similarity in the Fermi surfaces gives us confidence that for  $\text{Li}_x(\text{C}_3\text{N}_2\text{H}_{10})_{0.5}\text{FeSe}$ , we can avoid the difficulties of bulk FeSe where size and symmetry of Fermi surfaces are captured neither by DFT nor its extensions. Note, also, that DFT + DMFT, as applied in Ref. [22], has only a small effect on the Fermi surface of  $\text{Li}_x(\text{C}_3\text{N}_2\text{H}_{10})_{0.5}\text{FeSe}$ . Thus, the DFT Fermi surfaces are a reasonable starting point for the description of the material.

We would like to stress that we take advantage of the fact that in contrast to bulk FeSe where superconductivity develops out of a paramagnetic nematic phase with strong fluctuating magnetic moments which is not fully captured by DFT or DFT + DMFT, magnetic tendencies of FeSe intercalates are more conventional and therefore amenable to the electronic structure methods we employ here.

The dominant feature in the Fermi surface evolution with doping is the strong growth of the large angular electron pockets around the  $X$  and  $Y$  points in the one iron Brillouin zone (BZ). They have combined  $d_{xy}$  and  $d_{xz}/d_{yz}$  character. The hole pocket with  $d_{xy}$  character at the  $M$  point in the one iron BZ is rather insensitive to doping. Finally, several Lifshitz transitions occur around  $\Gamma$  with doping, as expected for an iron-based superconductor and previously noted in Ref. [22]. In a doping range of  $0.24 < x < 0.30$ , an inner hole pocket disappears, an outer hole pocket disappears, and an electron pocket appears; all these are of  $d_{xz}/d_{yz}$  character. The appearance of an electron pocket at  $\Gamma$  with doping has also been observed with ARPES on a potassium coated FeSe monolayer [56]. Without diaminopropane molecule, the Lifshitz transitions are spread over a range  $0.17 < x < 0.38$ , in reasonable agreement with the DFT calculations of Ref. [22].

The main effect on the density of states at the Fermi level  $N(E_F)$  (shown in Ref. [51], Fig. S4) is a 30% reduction around  $x = 0.27$  (or  $x = 0.35$  in the calculation without  $C_3N_2H_{10}$ ), which results from the disappearance of the two hole pockets; the appearance of the small electron pocket and its growth with doping helps  $N(E_F)$  to recover.

In the series of calculations without  $C_3N_2H_{10}$  molecule, we observe a doping range  $0.55 < x < 0.62$ , where the Fermi level is pinned to a band crossing. Topological properties of iron-based superconductors have recently been discussed intensively [57–60]. The presence of diaminopropane molecules in a fixed position as shown in Fig. 1(a) breaks the  $P4/nmm$  symmetry of  $Li_xFeSe$  and leads to the opening of a small gap in the band crossing. The high symmetry may be restored on average due to the statistical distribution of molecules in the high symmetry of the  $P4_212$  space group observed experimentally. Further theory and experiments are required to determine the nature of  $Li_x(C_3N_2H_{10})_{0.5}FeSe$  in the doping range  $0.55 < x < 0.62$ . As the unfolding does not capture the  $N(E_F)$  suppression in this doping range, we exclude it from our present discussion.

We now proceed to the spin fluctuation analysis by calculating the RPA spin and charge susceptibilities. As a representative example, we show in Fig. 3 the diagonal components  $\chi_{xy}^s$  and  $\chi_{yz}^s$  for the structures with  $C_3N_2H_{10}$  molecule. At low doping, the diagonal element  $\chi_{xy}^s$  [Fig. 3(a)] is dominated by a peak close to  $X$  and a minor peak close to  $M$ . These correspond to a nesting vector  $\mathbf{Q} = (\pi + \delta_x, 0 + \delta_y, q_z)$  connecting the electron pocket around  $X/Y$  and the hole pocket around the  $M$  point, and a nesting vector  $\mathbf{Q} = (\pi + \delta_x, \pi + \delta_y, q_z)$  connecting the electron pocket around  $X$  and that around  $Y$ . Furthermore,  $\chi_{yz}^s$  has a peak around  $X$ , which corresponds to a nesting vector  $\mathbf{Q} = (\pi + \delta_x, 0 + \delta_y, q_z)$  connecting the hole pocket around  $\Gamma$  and the electron pocket around  $X$ . The nesting vectors change with  $\delta_x, \delta_y$  because the electron pockets around  $X/Y$  grow. In both cases, the susceptibility peak formerly close to  $X$  progressively evolves towards  $\mathbf{Q} =$

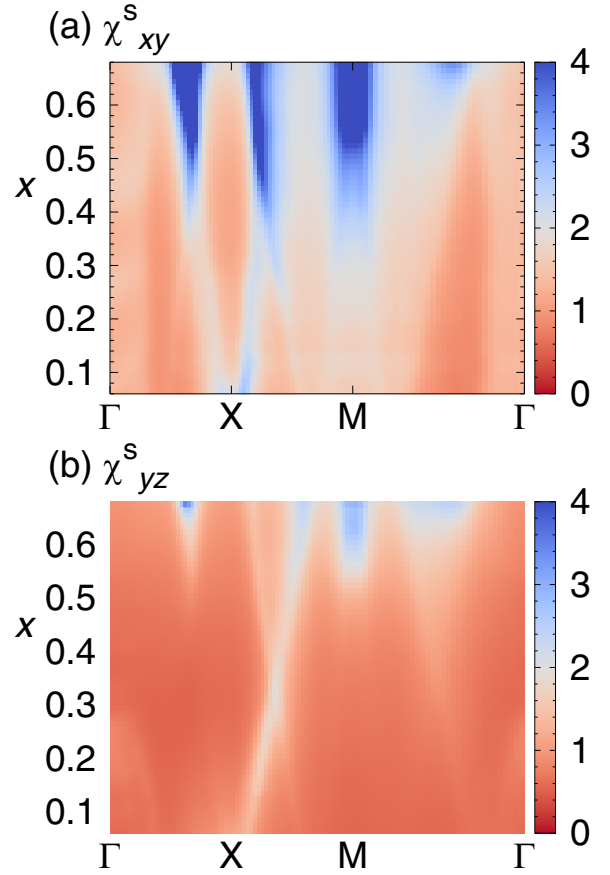


FIG. 3. Diagonal elements of the spin susceptibility as a function of momentum vector and doping.

$(\pi, \pi/2, q_z)$  with increasing doping. This tendency is further accentuated by the Lifshitz transition in the range  $0.24 < x < 0.30$ , which also rotates the orbital weights on the  $d_{xz}/d_{yz}$  hole pockets around  $\Gamma$  by 90 degrees.

Overall, we see an increase in both susceptibilities with doping. This is in line with the upward trend of  $N(E_F)$  which is interrupted by the loss of hole pockets around  $x = 0.27$  and by the band crossing pinned to the Fermi level for  $0.55 < x < 0.62$ . In agreement with this observation, the trend of the eigenvalue  $\lambda$  of the linearized gap equation as shown in Fig. 4 is an increase over the entire doping range, with the exception of  $x = 0.36$  where the Lifshitz transitions cause an abrupt drop of  $\lambda$ . The leading instabilities are different types of sign changing  $s$  wave in the whole region.

Clearly, the itinerant electron analysis of superconductivity in  $Li_x(C_3N_2H_{10})_{0.5}FeSe$  presented so far can be used to explain the increasing  $T_c$  up to  $x = 0.37$  observed in Ref. [22] (replotted for convenience in Ref. [51], Fig. S5) but not its suppression for higher doping. As an alternative, we now turn to the localized magnetic moment nature of the Fe  $3d$  electrons to search for a mechanism to suppress superconductivity. Figure 5 shows the first three in-plane exchange couplings of  $Li_x(C_3N_2H_{10})_{0.5}FeSe$  determined by energy mapping. The inspection of Heisenberg Hamiltonian parameters at this point should not be confused with the assumption of a magnetic ground state; rather, the purpose here is the analysis of the

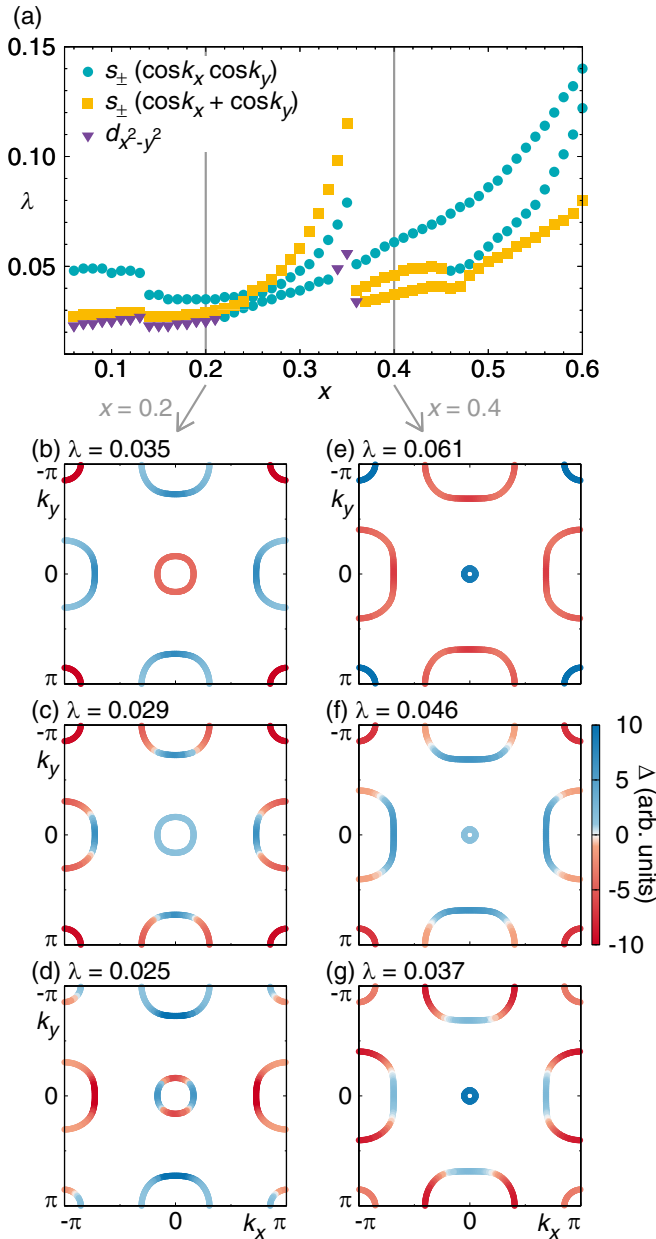


FIG. 4. (a) Leading eigenvalues  $\lambda$  of the gap equation as a function of doping level  $x$ . A jump is visible between  $x = 0.35$  and  $x = 0.36$ , where both of the hole pockets around  $\Gamma$  disappear due to a Lifshitz transition. (b)–(d) Leading gap functions on the Fermi surface at doping  $x = 0.20$ . (e)–(g) The same at doping  $x = 0.40$ . All of the results are obtained by calculations without  $C_3N_2H_{10}$ .

nature of the spin excitations out of which superconductivity is realized.

We find a smooth evolution of exchange couplings over the entire doping range. At small doping, the system starts with all couplings antiferromagnetic,  $J_2 = 0.61J_1$  and  $J_3$  nearly negligible. This makes the leading magnetic instability stripe-type AFM [51], in perfect agreement with the weak coupling evidence of peaks at  $X$  in the spin susceptibility  $\chi^s$  (Fig. 3). As doping increases,  $J_1$  decreases more rapidly than  $J_2$  so that at  $x = 0.33$ ,  $J_1$  and  $J_2$  coincide. This evolution strengthens the stripe-type AFM instability. However, the decrease of  $J_1$

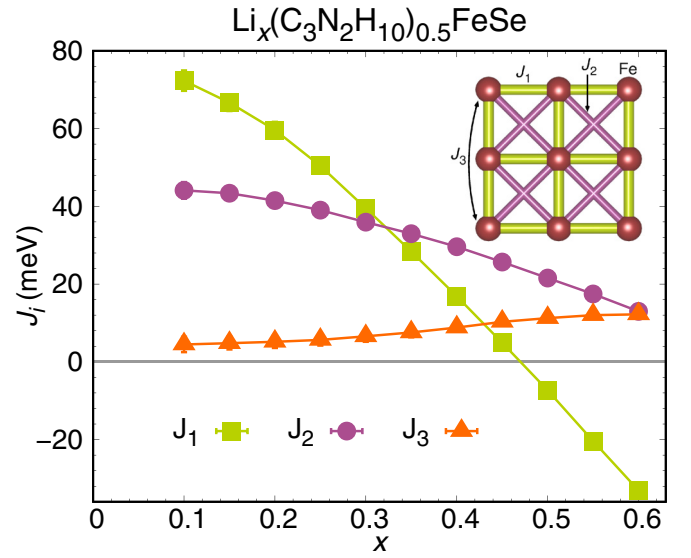


FIG. 5. Evolution of three in-plane exchange couplings of  $Li_x(C_3N_2H_{10})_{0.5}FeSe$  as a function of doping  $x$ , obtained from the energy mapping technique. The inset shows the three exchange paths on the iron square lattice.

accelerates until at  $x = 0.47$ ,  $J_1$  crosses zero and becomes ferromagnetic. Meanwhile,  $J_3$  is gradually increasing until at  $x = 0.6$ , it becomes as large as  $J_2$ . With FM  $J_1$  and substantial AFM  $J_3$ , bicollinear AFM has taken over as leading magnetic instability of  $Li_x(C_3N_2H_{10})_{0.5}FeSe$  (see Ref. [51], Figs. S6 and S7). Note that in the strongly doped region, the spin susceptibilities in Fig. 3 do show a peak close to  $Q = (\pi/2, \pi/2, 0)$  corresponding to the bicollinear order, but as this is not the dominant instability, the Heisenberg Hamiltonian cannot be understood based on the Fermi surface alone.

The bicollinear state is the magnetic ground state of FeTe, and as optimally doped  $FeTe_{1-x}Se_x$  has a  $T_c$  of only 14.5 K [61], our calculation provides a strong rationalization of the falling  $T_c$  as the magnetism of  $Li_x(C_3N_2H_{10})_{0.5}FeSe$  becomes more and more like that of FeTe. We identify the ferromagnetic tendencies of the nearest neighbor exchange as the key factor for determining the  $T_c$  evolution on the high doping side of the superconducting dome, outplaying all weak coupling effects of growing Fermi surfaces and growing density of states at the Fermi level.

Note that a similar transition of  $J_1$  from AFM to FM was found for a theoretical substitution series between iron pnictides and iron germanides [41], where superconductivity is in fact suppressed in the germanide. It is an interesting open question if the effect of ferromagnetic nearest neighbor interactions and thus a downward trend in  $T_c$  under electron doping could be captured in frequency dependent weak coupling methods like the fluctuation exchange approximation [36].

**Conclusions.** We have analyzed the superconductivity of  $Li_x(C_3N_2H_{10})_{0.5}FeSe$  as a function of doping in the range  $0.06 \leq x \leq 0.68$  both from itinerant electron and localized moment perspectives. We find that on the low doping side  $x \leq 0.37$ , growing Fermi surfaces and densities of states

at the Fermi level are the basis for explaining growing  $T_c$  with spin fluctuation theory. For higher doping level, weak coupling arguments would lead to the erroneous conclusion that  $T_c$  should continue to grow. However, the progressive destabilization of stripe type AFM fluctuations toward bicolinear antiferromagnetism explains why  $T_c$  decreases for  $x > 0.37$ .  $\text{Li}_x(\text{C}_3\text{N}_2\text{H}_{10})_{0.5}\text{FeSe}$  turns out to be a perfect demonstration of the fact that iron-based superconductivity can only be understood by fully accounting for itinerant and localized aspects of the Fe  $3d$  electrons. Our study highlights that in  $\text{Li}_x(\text{C}_3\text{N}_2\text{H}_{10})_{0.5}\text{FeSe}$ , as in many

strongly correlated materials, superconductivity develops out of magnetic interactions that are high energy, not Fermi surface properties, and treating this important class of materials quantitatively calls for further refinement of theoretical methods.

*Acknowledgments.* The authors would like to thank Hiroaki Kusunose and Igor Mazin for valuable discussions. Part of the computations were carried out at the Supercomputer Center at the Institute for Solid State Physics, the University of Tokyo. This work was supported by MEXT Leading Initiative for Excellent Young Researchers.

- [1] Yu. V. Pustovit and A. A. Kordyuk, Metamorphoses of electronic structure of FeSe-based superconductors, *Low Temp. Phys.* **42**, 995 (2016).
- [2] A. E. Böhrner and A. Kreisel, Nematicity, magnetism and superconductivity in FeSe, *J. Phys.: Condens. Matter* **30**, 023001 (2018).
- [3] A. I. Coldea and M. D. Watson, The Key Ingredients of the Electronic Structure of FeSe, *Annu. Rev. Condens. Matter Phys.* **9**, 125 (2018).
- [4] T. M. McQueen, A. J. Williams, P. W. Stephens, J. Tao, Y. Zhu, V. Ksenofontov, F. Casper, C. Felser, and R. J. Cava, Tetragonal-to-Orthorhombic Structural Phase Transition at 90 K in the Superconductor  $\text{Fe}_{1.01}\text{Se}$ , *Phys. Rev. Lett.* **103**, 057002 (2009).
- [5] M. Yi, H. Pfau, Y. Zhang, Y. He, H. Wu, T. Chen, Z. R. Ye, M. Hashimoto, R. Yu, Q. Si, D.-H. Lee, P. Dai, Z.-X. Shen, D. H. Lu, and R. J. Birgeneau, Nematic Energy Scale and the Missing Electron Pocket in FeSe, *Phys. Rev. X* **9**, 041049 (2019).
- [6] F.-C. Hsu, J.-Y. Luo, K.-W. Yeh, T.-K. Chen, T.-W. Huang, P. M. Wu, Y.-C. Lee, Y.-L. Huang, Y.-Y. Chu, D.-C. Yan, and M.-K. Wu, Superconductivity in the PbO-type structure  $\alpha$ -FeSe, *Proc. Natl. Acad. Sci. USA* **105**, 14262 (2008).
- [7] E.-W. Scheidt, V. R. Hathwar, D. Schmitz, A. Dunbar, W. Scherer, F. Mayr, V. Tsurkan, J. Deisenhofer, and A. Loidl, Superconductivity at  $T_c = 44$  K in  $\text{Li}_x\text{Fe}_2\text{Se}_2(\text{NH}_3)_y$ , *Eur. Phys. J. B* **85**, 279 (2012).
- [8] M. Burrard-Lucas, D. G. Free, S. J. Sedlmaier, J. D. Wright, S. J. Cassidy, Y. Hara, A. J. Corkett, T. Lancaster, P. J. Baker, S. J. Blundell, and S. J. Clarke, Enhancement of the superconducting transition temperature of FeSe by intercalation of a molecular spacer layer, *Nat. Mater.* **12**, 15 (2013).
- [9] S. J. Sedlmaier, S. J. Cassidy, R. G. Morris, M. Drakopoulos, C. Reinhard, S. J. Moorhouse, D. O'Hare, P. Manuel, D. Khalyavin, and S. J. Clarke, Ammonia-Rich High-Temperature Superconducting Intercalates of Iron Selenide Revealed through Time-Resolved in Situ X-ray and Neutron Diffraction, *J. Am. Chem. Soc.* **136**, 630 (2014).
- [10] P. Shahi, J. P. Sun, S. H. Wang, Y. Y. Jiao, K. Y. Chen, S. S. Sun, H. C. Lei, Y. Uwatoko, B. S. Wang, and J.-G. Cheng, High- $T_c$  superconductivity up to 55 K under high pressure in a heavily electron doped  $\text{Li}_{0.36}(\text{NH}_3)_y\text{Fe}_2\text{Se}_2$  single crystal, *Phys. Rev. B* **97**, 020508(R) (2018).
- [11] W. Bao, G.-N. Li, Q.-Z. Huang, G.-F. Chen, J.-B. He, D.-M. Wang, M. A. Green, Y.-M. Qiu, J.-L. Luo, and M.-M. Wu, Superconductivity tuned by the iron vacancy order in  $\text{K}_x\text{Fe}_{2-y}\text{Se}_2$ , *Chin. Phys. Lett.* **30**, 027402 (2013).
- [12] A. Krzton-Maziopa, V. Svitlyk, E. Pomjakushina, R. Puzniak, and K. Conder, Superconductivity in alkali metal intercalated iron selenides, *J. Phys. Condens. Matter* **28**, 293002 (2016).
- [13] H. Sun, D. N. Woodruff, S. J. Cassidy, G. M. Allcroft, S. J. Sedlmaier, A. L. Thompson, P. A. Bingham, S. D. Forder, S. Cartenet, N. Mary, S. Ramos, F. R. Foronda, B. J. Williams, X. Li, S. J. Blundell, and S. J. Clarke, Soft chemical control of superconductivity in lithium iron selenide hydroxides  $\text{Li}_{1-x}\text{Fe}_x(\text{OH})\text{Fe}_{1-y}\text{Se}$ , *Inorg. Chem.* **54**, 1958 (2015).
- [14] X. F. Lu, N. Z. Wang, H. Wu, Y. P. Wu, D. Zhao, X. Z. Zeng, X. G. Luo, T. Wu, W. Bao, G. H. Zhang, F. Q. Huang, Q. Z. Huang, and X. H. Chen, Coexistence of superconductivity and antiferromagnetism in  $(\text{Li}_{0.8}\text{Fe}_{0.2})\text{OHFeSe}$ , *Nat. Mater.* **14**, 325 (2015).
- [15] T. Noji, T. Hatakeda, S. Hosono, T. Kawamata, M. Kato, and Y. Koike, Synthesis and post-annealing effects of alkaline-metal-ethylenediamine intercalated superconductors  $\text{A}_x(\text{C}_2\text{H}_8\text{N}_2)_y\text{Fe}_{2-z}\text{Se}_2$  ( $\text{A} = \text{Li}, \text{Na}$ ) with  $T_c = 45$  K, *Physica C* **504**, 8 (2014).
- [16] X. Zhou, C. Eckberg, B. Wilfong, S.-C. Liou, H. K. Vivanco, J. Paglione, and E. E. Rodriguez, Superconductivity and magnetism in iron sulfides intercalated by metal hydroxides, *Chem. Sci.* **8**, 3781 (2017).
- [17] L. Zheng, Y. Sakai, X. Miao, S. Nishiyama, T. Terao, R. Eguchi, H. Goto, and Y. Kubozono, Superconductivity in  $(\text{NH}_3)_y\text{Na}_x\text{FeSe}_{0.5}\text{Te}_{0.5}$ , *Phys. Rev. B* **94**, 174505 (2016).
- [18] C. Li, S. Su, S. Wang, and H. Lei, Enhanced superconductivity and anisotropy of  $\text{FeTe}_{0.6}\text{Se}_{0.4}$  single crystals with  $\text{Li-NH}_3$  intercalation, *Phys. Rev. B* **96**, 134503 (2017).
- [19] S. Medvedev, T. M. McQueen, I. A. Troyan, T. Palasyuk, M. I. Erements, R. J. Cava, S. Naghavi, F. Casper, V. Ksenofontov, G. Wortmann, and C. Felser, Electronic and magnetic phase diagram of  $\beta$ - $\text{Fe}_{1.01}\text{Se}$  with superconductivity at 36.7 K under pressure, *Nat. Mater.* **8**, 630 (2009).
- [20] S. Jin, X. Fan, X. Wu, R. Sun, H. Wu, Q. Huang, C. Shi, X. Xi, Z. Lia, and X. Chen, High- $T_c$  superconducting phases in organic molecular intercalated iron selenides: synthesis and crystal structures, *Chem. Commun.* **53**, 9729 (2017).
- [21] T. Hatakeda, T. Noji, K. Sato, T. Kawamata, M. Kato, and Y. Koike, New alkali-metal- and 2-phenethylamine-intercalated superconductors  $\text{A}_x(\text{C}_8\text{H}_{11}\text{N})_y\text{Fe}_{1-z}\text{Se}$  ( $\text{A} = \text{Li}, \text{Na}$ ) with the

- Largest Interlayer Spacings and  $T_c \sim 40$  K, *J. Phys. Soc. Jpn.* **85**, 103702 (2016).
- [22] R. J. Sun, Y. Quan, S. F. Jin, Q. Z. Huang, H. Wu, L. Zhao, L. Gu, Z. P. Yin, and X. L. Chen, Realization of continuous electron doping in bulk iron selenides and identification of a new superconducting zone, *Phys. Rev. B* **98**, 214508 (2018).
- [23] S. Hosono, T. Noji, T. Hatakeda, T. Kawamata, M. Kato, and Y. Koike, New Intercalation Superconductor  $\text{Li}_x(\text{C}_6\text{H}_{16}\text{N}_2)_y\text{Fe}_{2-z}\text{Se}_2$  with a Very Large Interlayer-Spacing and  $T_c = 38$  K, *J. Phys. Soc. Jpn.* **83**, 113704 (2014).
- [24] S. Hosono, T. Noji, T. Hatakeda, T. Kawamata, M. Kato, and Y. Koike, New superconducting phase of  $\text{Li}_x(\text{C}_6\text{H}_{16}\text{N}_2)_y\text{Fe}_{2-z}\text{Se}_2$  with  $T_c = 41$  K obtained through the post-annealing, *J. Phys. Soc. Jpn.* **85**, 013702 (2016).
- [25] L. Sun, X.-J. Chen, J. Guo, P. Gao, Q.-Z. Huang, H. Wang, M. Fang, X. Chen, G. Chen, Q. Wu, C. Zhang, D. Gu, X. Dong, L. Wang, K. Yang, A. Li, X. Dai, H.-K. Mao, and Z. Zhao, Re-emerging superconductivity at 48 Kelvin in iron chalcogenides, *Nature (London)* **483**, 67 (2012).
- [26] M. Izumi, L. Zheng, Y. Sakai, H. Goto, M. Sakata, Y. Nakamoto, H. L. T. Nguyen, T. Kagayama, K. Shimizu, S. Araki, T. C. Kobayashi, T. Kambe, D. Gu, J. Guo, J. Liu, Y. Li, L. Sun, K. Prassides, and Y. Kubozono, Emergence of double-dome superconductivity in ammoniated metal-doped FeSe, *Sci. Rep.* **5**, 9477 (2015).
- [27] C.-L. Song, H.-M. Zhang, Y. Zhong, X.-P. Hu, S.-H. Ji, L. Wang, K. He, X.-C. Ma, and Q.-K. Xue, Observation of Double-Dome Superconductivity in Potassium-Doped FeSe Thin Films, *Phys. Rev. Lett.* **116**, 157001 (2016).
- [28] J. P. Sun, P. Shahi, H. X. Zhou, Y. L. Huang, K. Y. Chen, B. S. Wang, S. L. Ni, N. N. Li, K. Zhang, W. G. Yang, Y. Uwatoko, G. Xing, J. Sun, D. J. Singh, K. Jin, F. Zhou, G. M. Zhang, X. L. Dong, Z. X. Zhao, and J.-G. Cheng, Reemergence of high- $T_c$  superconductivity in the  $(\text{Li}_{1-x}\text{Fe}_x)\text{OHFe}_{1-y}\text{Se}$  under high pressure, *Nat. Commun.* **9**, 380 (2018).
- [29] J. Zhang, F.-L. Liu, T.-P. Ying, N.-N. Li, Y. Xu, L.-P. He, X.-C. Hong, Y.-J. Yu, M.-X. Wang, J. Shen, W.-G. Yang, and S.-Y. Li, Observation of two superconducting domes under pressure in tetragonal FeS, *npj Quant. Mater.* **2**, 49 (2017).
- [30] I. I. Mazin, D. J. Singh, M. D. Johannes, and M. H. Du, Unconventional Superconductivity with a Sign Reversal in the Order Parameter of  $\text{LaFeAsO}_{1-x}\text{F}_x$ , *Phys. Rev. Lett.* **101**, 057003 (2008).
- [31] K. Kuroki, S. Onari, R. Arita, H. Usui, Y. Tanaka, H. Kontani, and H. Aoki, Unconventional Pairing Originating from the Disconnected Fermi Surfaces of Superconducting  $\text{LaFeAsO}_{1-x}\text{F}_x$ , *Phys. Rev. Lett.* **101**, 087004 (2008).
- [32] P. J. Hirschfeld, M. M. Korshunov, and I. I. Mazin, Gap symmetry and structure of Fe-based superconductors, *Rep. Prog. Phys.* **74**, 124508 (2011).
- [33] P. A. Lee, N. Nagaosa, and X.-G. Wen, Doping a Mott insulator: Physics of high-temperature superconductivity, *Rev. Mod. Phys.* **78**, 17 (2006).
- [34] Q. Si and E. Abrahams, Strong Correlations and Magnetic Frustration in the High  $T_c$  Iron Pnictides, *Phys. Rev. Lett.* **101**, 076401 (2008).
- [35] J. C. S. Davis and D.-H. Lee, Concepts relating magnetic interactions, intertwined electronic orders, and strongly correlated superconductivity, *Proc. Natl. Acad. Sci. USA* **110**, 17623 (2013).
- [36] K. Suzuki, H. Usui, S. Iimura, Y. Sato, S. Matsuishi, H. Hosono, and K. Kuroki, Model of the Electronic Structure of Electron-Doped Iron-Based Superconductors: Evidence for Enhanced Spin Fluctuations by Diagonal Electron Hopping, *Phys. Rev. Lett.* **113**, 027002 (2014).
- [37] D. Guterding, H. O. Jeschke, P. J. Hirschfeld, and R. Valentí, Unified picture of the doping dependence of superconducting transition temperatures in alkali metal/ammonia intercalated FeSe, *Phys. Rev. B* **91**, 041112(R) (2015).
- [38] M. Shimizu, N. Takemori, D. Guterding, and H. O. Jeschke, Two-Dome Superconductivity in FeS Induced by a Lifshitz Transition, *Phys. Rev. Lett.* **121**, 137001 (2018).
- [39] J. Hu, H. Ding, Local antiferromagnetic exchange and collaborative Fermi surface as key ingredients of high temperature superconductors, *Sci. Rep.* **2**, 381 (2012).
- [40] J. K. Glasbrenner, I. I. Mazin, H. O. Jeschke, P. J. Hirschfeld, R. M. Fernandes, and R. Valentí, Effect of magnetic frustration on nematicity and superconductivity in iron chalcogenides, *Nat. Phys.* **11**, 953 (2015).
- [41] D. Guterding, H. O. Jeschke, I. I. Mazin, J. K. Glasbrenner, E. Bascones, and R. Valentí, Nontrivial Role of Interlayer Cation States in Iron-Based Superconductors, *Phys. Rev. Lett.* **118**, 017204 (2017).
- [42] K. Koepf and H. Eschrig, Full-potential nonorthogonal local-orbital minimum-basis band-structure scheme, *Phys. Rev. B* **59**, 1743 (1999); <http://www.FPLO.de>.
- [43] J. P. Perdew, K. Burke, and M. Ernzerhof, Generalized Gradient Approximation Made Simple, *Phys. Rev. Lett.* **77**, 3865 (1996).
- [44] H. Eschrig and K. Koepf, Tight-binding models for the iron-based superconductors, *Phys. Rev. B* **80**, 104503 (2009).
- [45] M. Tomić, H. O. Jeschke, and R. Valentí, Unfolding of electronic structure through induced representations of space groups: Application to Fe-based superconductors, *Phys. Rev. B* **90**, 195121 (2014).
- [46] S. Graser, T. A. Maier, P. J. Hirschfeld, and D. J. Scalapino, Near-degeneracy of several pairing channels in multiorbital models for the Fe pnictides, *New J. Phys.* **11**, 025016 (2009).
- [47] D. Guterding, Microscopic modeling of organic and iron-based superconductors, PhD. thesis, Goethe-Universität Frankfurt am Main, Germany, 2017.
- [48] H. O. Jeschke, H. Nakano, and T. Sakai, From kagome strip to kagome lattice: Realizations of frustrated  $S = 1/2$  antiferromagnets in Ti(III) fluorides, *Phys. Rev. B* **99**, 140410 (2019).
- [49] I. I. Mazin, M. Shimizu, N. Takemori, and H. O. Jeschke, Novel Fe-Based Superconductor  $\text{LaFe}_2\text{As}_2$  in Comparison with Traditional Pnictides, *Phys. Rev. Lett.* **123**, 267001 (2019).
- [50] M. F. Lapa and C. L. Henley, Ground States of the Classical Antiferromagnet on the Pyrochlore Lattice, [arXiv:1210.6810](https://arxiv.org/abs/1210.6810).
- [51] See Supplemental Material at <http://link.aps.org/supplemental/10.1103/PhysRevB.101.180511> for details on the crystal structures, the electronic properties, the energy mapping, and the iterative minimization calculations, which includes Refs. [52–54].
- [52] H. O. Jeschke, I. Opahle, H. Kandpal, R. Valentí, H. Das, T. Saha-Dasgupta, O. Janson, H. Rosner, A. Brühl, B. Wolf, M. Lang, J. Richter, S. Hu, X. Wang, R. Peters, T. Pruschke, and A. Honecker, Multi-Step Approach to Microscopic Models for Frustrated Quantum Magnets: The Case of the Natural Mineral Azurite, *Phys. Rev. Lett.* **106**, 217201 (2011).

- [53] Y. Iqbal, T. Müller, K. Riedl, J. Reuther, S. Rachel, R. Valentí, M. J. P. Gingras, R. Thomale, and H. O. Jeschke, Signatures of a gearwheel quantum spin liquid in a spin- $1/2$  pyrochlore molybdate Heisenberg antiferromagnet, *Phys. Rev. Mater.* **1**, 071201(R) (2017).
- [54] Y. Iqbal, T. Müller, H. O. Jeschke, R. Thomale, and J. Reuther, Stability of the spiral spin liquid in  $\text{MnSc}_2\text{S}_4$ , *Phys. Rev. B* **98**, 064427 (2018).
- [55] L. Zhao, A. Liang, D. Yuan, Y. Hu, D. Liu, J. Huang, S. He, B. Shen, Y. Xu, X. Liu, L. Yu, G. Liu, H. Zhou, Y. Huang, X. Dong, F. Zhou, K. Liu, Z. Lu, Z. Zhao, C. Chen, Z. Xu, and X. J. Zhou, Common electronic origin of superconductivity in (Li, Fe)OHFeSe bulk superconductor and single-layer FeSe/SrTiO<sub>3</sub> films, *Nat. Commun.* **7**, 10608 (2016).
- [56] X. Shi, Z.-Q. Han, X.-L. Peng, P. Richard, T. Qian, X.-X. Wu, M.-W. Qiu, S. C. Wang, J. P. Hu, Y.-J. Sun, and H. Ding, Enhanced superconductivity accompanying a Lifshitz transition in electron-doped FeSe monolayer, *Nat. Commun.* **8**, 14988 (2017).
- [57] X. Wu, S. Qin, Y. Liang, H. Fan, and J. Hu, Topological Characters in  $\text{Fe}(\text{Te}_{1-x}\text{Se}_x)$  thin films, *Phys. Rev. B* **93**, 115129 (2016).
- [58] G. Xu, B. Lian, P. Tang, X.-L. Qi, and S.-C. Zhang, Topological Superconductivity on the Surface of Fe-Based Superconductors, *Phys. Rev. Lett.* **117**, 047001 (2016).
- [59] P. Zhang, K. Yaji, T. Hashimoto, Y. Ota, T. Kondo, K. Okazaki, Z. Wang, J. Wen, G. D. Gu, H. Ding, and S. Shin, Observation of topological superconductivity on the surface of an iron-based superconductor, *Science* **360**, 182 (2018).
- [60] D. Wang, L. Kong, P. Fan, H. Chen, S. Zhu, W. Liu, L. Cao, Y. Sun, S. Du, J. Schneeloch, R. Zhong, G. Gu, L. Fu, H. Ding, and H.-J. Gao, Evidence for Majorana bound states in an iron-based superconductor, *Science* **362**, 333 (2018).
- [61] N. Katayama, S. Ji, D. Louca, S. Lee, M. Fujita, T. J. Sato, J. Wen, Z. Xu, G. Gu, G. Xu, Z. Lin, M. Enoki, S. Chang, K. Yamada, and J. M. Tranquada, Investigation of the spin-glass regime between the antiferromagnetic and superconducting phases in  $\text{Fe}_{1+y}\text{Se}_x\text{Te}_{1-x}$ , *J. Phys. Soc. Jpn.* **79**, 113702 (2010).